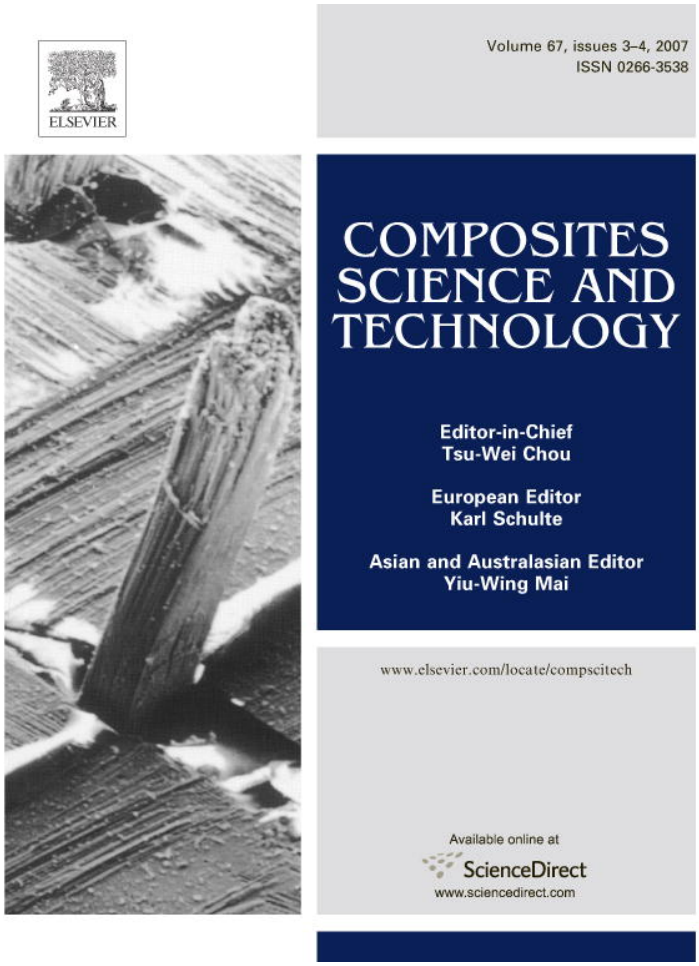

Available online at www.sciencedirect.com
ScienceDirect
Composites Science and Technology 67 (2007) 489–500
COMPOSITES SCIENCE AND TECHNOLOGY
www.elsevier.com/locate/compscitech

Out-of-plane behavior of unreinforced masonry walls strengthened with FRP strips

E. Hamed [1], O. Rabinovitch [*,2]

Technion-Israel Institute of Technology, Faculty of Civil and Environmental Engineering, Haifa 32000, Israel

Received 29 December 2005; received in revised form 20 August 2006; accepted 24 August 2006
Available online 19 October 2006

Abstract

The out-of-plane behavior of unreinforced masonry walls strengthened with externally bonded fiber reinforced polymer (FRP) strips is analytically studied. The analytical model uses variational principles, equilibrium requirements, and compatibility conditions between the structural components (masonry units, mortar joints, FRP strips, and adhesive layers) and assumes one-way flexural action of the strengthened wall. The masonry units and the mortar joints are modeled as Timoshenko's beams. The FRP strips are modeled using the lamination and the first-order shear deformation theories, and the adhesive layers are modeled as 2D linear elastic continua. The model accounts for cracking of the mortar joints and for the development of debonding zones near the cracked joints. Numerical and parametric studies that reveal the capabilities of the model, throw light on the interaction between the variables, and quantitatively explain some aspects of the behavior of the strengthened wall are also presented.

Keywords: Bonding; Composite materials; C. Cracking; C. Delamination; Masonry; Strengthening; Structural analysis

1. Introduction

Unreinforced masonry (URM) walls are used in a broad range of historic and modern buildings worldwide. Nevertheless, these members are vulnerable to out-of-plane loads such as soil pressure, lateral fluid pressure, wind loads, seismic loads, and others. In severe cases, the out-of-plane loading may lead to loss of functionality of the wall, structural damage, or even total failure [1]. In other cases, and especially in historic masonry buildings, these effects may weaken the entire structural assembly. These issues highlight the need for efficient strengthening of the URM wall.

Among the techniques available today for the strengthening of URM walls, the use of externally bonded fiber reinforced polymer (FRP) has been designated as an attractive structural solution [2,3]. Experimental investigations showed that the use of the externally bonded FRP laminates leads to an increase of up to 50 times in the strength of the masonry wall [4]. In addition, and opposed to RC beams [5,6], the bonded laminates enhance the ductility of the strengthened masonry wall and provide it with the ability to dissipate energy by cracking of the joints [7].

Along with the improved stiffness, strength, and ductility, the experimental studies also revealed a broad range of physical phenomena that characterize the behavior of the strengthened wall [8–14]. These unique physical phenomena include rupture of the FRP strip or crushing of the masonry at the mortar joints; debonding of the FRP strip; sliding of the masonry units (mortar slip); flexural-shear cracking near the corners of the masonry unit; and outward buckling/wrinkling of the compressed FRP strip. Many of these phenomena are unique to the strengthened masonry wall and have not been observed in RC beams and slabs strengthened with FRP strips.

The scope of the analytical models that address the behavior of the strengthened URM wall is rather limited.

* Corresponding author. Tel.: +972 4 8293047; fax: +972 4 8295697.
E-mail address: cvoded@tx.technion.ac.il (O. Rabinovitch).
[1] Ph.D. Student.
[2] Senior Lecturer and Horev Fellow, supported by the Taub Foundation.

0266-3538/$ - see front matter © 2006 Elsevier Ltd. All rights reserved.
doi:10.1016/j.compscitech.2006.08.021

Hamilton and Dolan [8], Hamoush et al. [10] and Velazquea-Dimas and Ehsani [15] used the strain compatibility approach for the analysis of externally bonded masonry walls. This model can describe the overall load–deflection behavior and can predict the ultimate load in cases of flexural failure by rupture of the FRP or crushing of the masonry units. However, the effect of debonding, the local phenomena near the joints and their influence on the global behavior of the strengthened wall are beyond its capabilities.

Kiss et al. [16] presented a fracture mechanics model for the delamination growth between the FRP sheet and the masonry panel. However, this model does not consider the critical development of the shear and peeling stresses at the masonry-FRP interface and their influence on the distribution of the internal forces and stresses within the strengthened wall. Cecchi et al. [17] proposed a homogenization approach for the out-of-plane analysis of strengthened masonry walls. This model does not account for the localized cracking of the mortar joints, which critically affects the global and local response of the wall. Hence, the validity of this approach is limited to the elastic range only. A preliminary approach for the bending response of strengthened masonry walls was described in Hamed and Rabinovitch [18]. This model neglects the initial tensile strength and shear deformability of the mortar material, and uses a uniform and presumed depth of the compression zone. As a result, it cannot describe the realistic cracking conditions at the joints and their development along the loading process.

Davidson et al. [14] used the FE method for the analysis of strengthened masonry walls. However, the different length scales (thickness of the adhesive layer and the FRP strip with respect to the thickness of the masonry unit), the differences in the mechanical properties, and the singularities and stress concentrations in critical locations make the FE analysis of the strengthened masonry wall complicated and computational effort consuming.

In this paper, the structural behavior of URM walls strengthened with externally bonded FRP strips to resist out-of-plane loading is analytically investigated. The goals of this study are to develop a theoretical approach for the structural analysis of the strengthened masonry wall and to gain insight into the physical phenomena that govern its behavior. The analytical model developed in the paper assumes a one-way flexural response of the strengthened wall. This behavior is attributed to the boundary conditions of the existing wall and to the strengthening technique with one-way FRP strips [14]. Each masonry unit and each mortar joint is modeled as first order shear deformable Timoshenko's beam [19], with special consideration of the cracking of the joints [8,15]. Following [20], the adhesive layers are modeled as two dimensional linear elastic continua with shear and out-of-plane normal rigidities only and the FRP strips are modeled using the lamination theory.

The assembly of the various components of the wall (masonry units, mortar joints, FRP strips, adhesive layers) into a whole structure is achieved through compatibility and continuity conditions. Perfect bonding and transfer of shear and normal stresses is assumed at the interfaces between the various components. However, in case the mortar joint is cracked or the masonry–mortar interface is partially detached and according to the experimental observations in [8,12,13], it is assumed that a localized debonded region where the adhesive-mortar interface cannot transfer shear stresses is formed. For simplicity, it is assumed that the debonded regions do not grow under loading and that the loads are exerted at the masonry panel only.

2. Mathematical formulation

The sign conventions for the coordinates, deformations, loads, stresses, and stress resultants of the unidirectionally strengthened masonry wall appear in Fig. 1. Following [8,21,22], it is assumed that the spacing between the FRP strips is sufficiently small to allow the development of a uniform compressive zone through the width of the wall. Thus, it is assumed that the stress and deformation fields are uniform through the width of each structural component. The strengthened masonry panel includes strengthened regions and unstrengthened regions near the external supports. The strengthened region itself includes two types of sub-regions, namely fully bonded sub-regions and debonded (delaminated) sub-regions near the cracked mortar joints. A further distinction is made between debonded sub-regions where the debonded interfaces maintain out-of-plane contact (and transfer normal compressive stresses), and debonded sub-regions without such contact. In both cases, it is assumed that the debonded interfaces are free of shear stresses.

The equilibrium equations and the boundary and continuity conditions are derived through the variational principle of virtual work, which requires that

$$\delta(U+V)=0 \tag{1}$$

where U is the strain energy, V is the potential of the external loads, and δ is the variational operator. The first variation of the strain energy is

$$\begin{aligned}\delta U = &\sum_{1}^{\mathrm{Nmu}} \int_{V_{\mathrm{mu}}} \left(\sigma_{xx}^{\mathrm{mu}}\delta\varepsilon_{xx}^{\mathrm{mu}} + \tau_{xz}^{\mathrm{mu}}\delta\gamma_{xz}^{\mathrm{mu}}\right) \mathrm{d}v_{\mathrm{mu}} \\ &+ \sum_{1}^{\mathrm{Nmj}} \int_{V_{\mathrm{mj}}} \left(\sigma_{xx}^{\mathrm{mj}}\delta\varepsilon_{xx}^{\mathrm{mj}} + \tau_{xz}^{\mathrm{mj}}\delta\gamma_{xz}^{\mathrm{mj}}\right) \mathrm{d}v_{\mathrm{mj}} \\ &+ \int_{V_{\mathrm{frp1}}} \left(\sigma_{xx}^{\mathrm{frp1}}\delta\varepsilon_{xx}^{\mathrm{frp1}} + \tau_{xz}^{\mathrm{frp1}}\delta\gamma_{xz}^{\mathrm{frp1}}\right) \mathrm{d}v_{\mathrm{frp1}} \\ &+ \int_{V_{\mathrm{frp2}}} \left(\sigma_{xx}^{\mathrm{frp2}}\delta\varepsilon_{xx}^{\mathrm{frp2}} + \tau_{xz}^{\mathrm{frp2}}\delta\gamma_{xz}^{\mathrm{frp2}}\right) \mathrm{d}v_{\mathrm{frp2}} \\ &+ \int_{V_{\mathrm{a1}}} \left(\tau_{xz}^{\mathrm{a1}}\delta\gamma_{xz}^{\mathrm{a1}} + \sigma_{zz}^{\mathrm{a1}}\delta\varepsilon_{zz}^{\mathrm{a1}}\right) \mathrm{d}v_{\mathrm{a1}} \\ &+ \int_{V_{\mathrm{a2}}} \left(\tau_{xz}^{\mathrm{a2}}\delta\gamma_{xz}^{\mathrm{a2}} + \sigma_{zz}^{\mathrm{a2}}\delta\varepsilon_{zz}^{\mathrm{a2}}\right) \mathrm{d}v_{\mathrm{a2}}\end{aligned} \tag{2}$$

where the superscripts mu, mj, frp1, frp2, a1 and a2 refer to the masonry unit, mortar, inner FRP strip, outer FRP

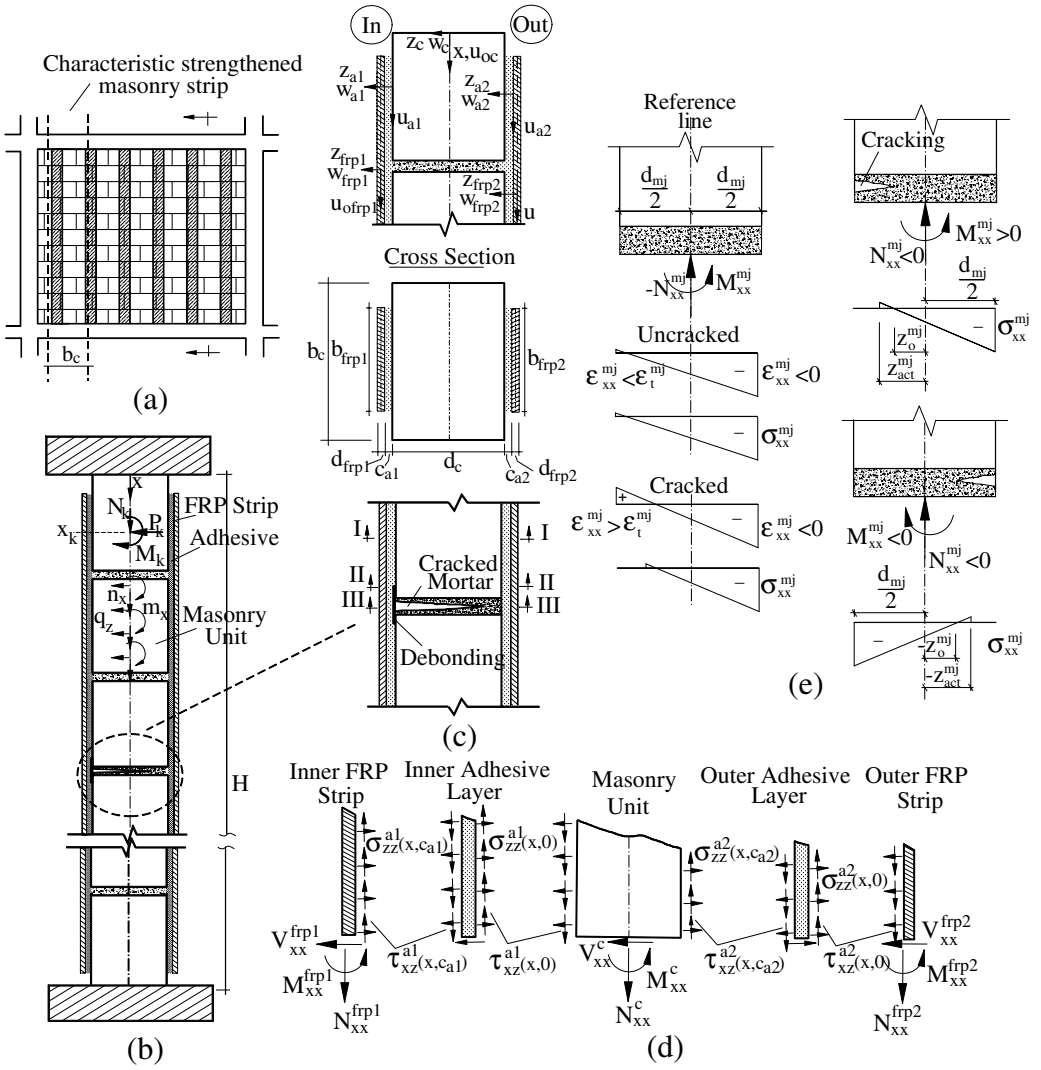

Fig. 1. Geometry, loads, sign conventions, and stresses: (a) masonry wall strengthened with FRP strips; (b) geometry and loads; (c) cracked joint, cross section, and notation; (d) stresses and stress resultants; (e) stress and strain distributions through the mortar join.

strip, inner adhesive layer, and the outer adhesive layer, respectively; σ^i_{xx} and ε^i_{xx} are the in-plane normal stress and strain in the masonry unit ($i=\text{mu}$), the mortar joint ($i=\text{mj}$), and the FRP strips ($i=\text{frp1}$ or $i=\text{frp2}$); τ^i_{xz} and γ^i_{xz} ($i=\text{mu},\text{mj},\text{frp1},\text{frp2},\text{a1},\text{a2}$) are the shear stresses and shear angles, respectively; σ^j_{zz} and ε^j_{zz} ($j=\text{a1},\text{a2}$) are the out-of-plane normal stresses and strains in the inner and the outer adhesive layers, respectively; and Nmu and Nmj are the number of the masonry units and the mortar joints, respectively.

The kinematic relations for the masonry units, the mortar joints, and the FRP strips follow the small displacements first order shear deformation theory:

$$\begin{aligned} w_i(x,z_i) &= w_i(x) \\ u_i(x,z_i) &= u_{oi}(x) - z_i\phi_i(x) \\ \gamma^i_{xz}(x,z_i) &= w_{i,x}(x) - \phi_i(x) \\ \varepsilon^i_{xx}(x,z_i) &= u_{oi,x}(x) - z_i\phi_{i,x}(x) \end{aligned} \tag{3a–d}$$

where w_i, u_{oi} and ϕ_i are the out-of-plane displacement, the in-plane displacement, and the rotation of the cross section of the masonry unit ($i=\text{mu}$), the mortar joint ($i=\text{mj}$), and the FRP strips ($i=\text{frp1},\text{frp2}$), and $()_{,x}$ denotes a derivative with respect to x. The reference line for each component is arbitrarily located at the *middle of its depth*, and z_i is measured from the reference line inwards (Fig. 1(c)). Since both the masonry units and the mortar joints are modeled using the Timoshenko's beam kinematics (and defer only in their constitutive behavior), the superscripts "mu" and "mj" are replaced with "c". Thus, $c=\text{mu}$ for the "masonry regions" (sections I–I and II–II in Fig. 1(c)), and $c=\text{mj}$ for the "mortar regions" (section III–III in Fig. 1(c)).

The kinematic relations for the adhesive are based on 2D linear elasticity:

$$\begin{aligned} \varepsilon^j_{zz}(x,z_j) &= w_{j,z}(x,z_j) \\ \gamma^j_{xz}(x,z_j) &= u_{j,z}(x,z_j) + w_{j,x}(x,z_j) \quad (j=\text{a1},\text{a2}) \end{aligned} \tag{4a, b}$$

where w_j and u_j are the out-of-plane and in-plane displacements of the inner ($j=\mathrm{a1}$) and outer ($j=\mathrm{a2}$) adhesive layers, respectively.

Assuming that the loads are exerted at the masonry wall only, the first variation of the potential of the external loads equals

$$\begin{aligned}\delta V = & -\int_{x=0}^{x=L}(q_z\delta w_c + n_x\delta u_{oc} + m_x\delta\phi_c)\\ & -\sum_{k=1}^{\mathrm{NC}}\int_{x=0}^{x=L}(P_k\delta w_c(x_k) + N_k\delta u_{oc}(x_k)\\ & + M_k\delta\phi_c(x_k))\delta_{\mathrm{D}}(x-x_k)\,\mathrm{d}x \end{aligned} \tag{5}$$

where q_z, n_x, and m_x are external distributed loads and bending moments, respectively, P_k, N_k, and M_k are concentrated loads and bending moments at $x=x_k$ (see Fig. 1(b)), δ_{D} is the Dirac function, and NC is the number of concentrated loads and moments.

2.1. Compatibility and debonding conditions

In case the strengthening system is fully bonded (“fully bonded” regions), the compatibility conditions at the interfaces of the adhesive layers are

$$w_{\mathrm{a1}}(x,z_{\mathrm{a1}}=0)=w_c(x)$$

$$u_{\mathrm{a1}}(x,z_{\mathrm{a1}}=0)=u_{oc}(x)-\frac{d_c}{2}\phi_c(x) \tag{6a, b}$$

$$w_{\mathrm{a1}}(x,z_{\mathrm{a1}}=c_{\mathrm{a1}})=w_{\mathrm{frp1}}(x)$$

$$u_{\mathrm{a1}}(x,z_{\mathrm{a1}}=c_{\mathrm{a1}})=u_{o\mathrm{frp1}}(x)+\frac{d_{\mathrm{frp1}}}{2}\phi_{\mathrm{frp1}}(x) \tag{7a, b}$$

$$w_{\mathrm{a2}}(x,z_{\mathrm{a2}}=0)=w_{\mathrm{frp2}}(x)$$

$$u_{\mathrm{a2}}(x,z_{\mathrm{a2}}=0)=u_{o\mathrm{frp2}}(x)-\frac{d_{\mathrm{frp2}}}{2}\phi_{\mathrm{frp2}}(x) \tag{8a, b}$$

$$w_{\mathrm{a2}}(x,z_{\mathrm{a2}}=c_{\mathrm{a2}})=w_c(x);$$

$$u_{\mathrm{a2}}(x,z_{\mathrm{a2}}=c_{\mathrm{a2}})=u_{oc}(x)+\frac{d_c}{2}\phi_c(x) \tag{9a, b}$$

where $d_c(=d_{\mathrm{mu}}$ or $d_{\mathrm{mj}})$, d_{frp1} and d_{frp2} are the thicknesses of the masonry unit, the mortar joint, and the FRP strips, respectively, c_{a1} and c_{a2} are the thicknesses of the inner and outer adhesive layers, respectively, and z_j ($j=\mathrm{a1},\mathrm{a2}$) are measured from the outer interface of each adhesive layer inwards, see Fig. 1(c).

If the adhesive interface is debonded, the requirement of compatible in-plane displacements is replaced with the condition of shear stress free surface. For example, if the inner adhesive-masonry interface is debonded, Eq. (6b) is replaced with

$$\tau^{\mathrm{a1}}_{xz}(x,z_{\mathrm{a1}}=0)=0 \tag{10}$$

In case out-of-plane contact exists, the debonded surfaces maintain out-of-plane compatibility (Eqs. (6a), (7a), (8a), and (9a)). If such contact does not exist, the out-of-plane compatibility condition is replaced with a zero out-of-plane normal stress condition. For example, in the case mentioned above, Eq. (6a) is replaced with

$$\sigma^{\mathrm{a1}}_{zz}(x,z_{\mathrm{a1}}=0)=0 \tag{11a, b}$$

2.2. Equilibrium equations

The equilibrium equations for the strengthened (bonded and debonded) regions are formulated using the variational principle (Eqs. 1,2,5), along with the kinematic relations (Eqs. (3) and (4)), and the compatibility requirements (Eqs. (6)–(11)), and they read

$$N^{\mathrm{frp1}}_{xx,x}(x)-\alpha^{\mathrm{frp}}_1 b_{\mathrm{frp1}}\tau^{\mathrm{a1}}_{xz}(x,z_{\mathrm{a1}}=c_{\mathrm{a1}})=0 \tag{12}$$

$$\begin{aligned}N^{c}_{xx,x}(x)-\alpha^{c}_2 b_{\mathrm{frp2}}\tau^{\mathrm{a2}}_{xz}(x,z_{\mathrm{a2}}=c_{\mathrm{a2}})\\ +\alpha^{c}_1 b_{\mathrm{frp1}}\tau^{\mathrm{a1}}_{xz}(x,z_{\mathrm{a1}}=0)=-n_x(x)\end{aligned} \tag{13}$$

$$N^{\mathrm{frp2}}_{xx,x}(x)+\alpha^{\mathrm{frp}}_2 b_{\mathrm{frp2}}\tau^{\mathrm{a2}}_{xz}(x,z_{\mathrm{a2}}=0)=0 \tag{14}$$

$$V^{\mathrm{frp1}}_{xx,x}(x)-\beta^{\mathrm{frp}}_1 b_{\mathrm{frp1}}\sigma^{\mathrm{a1}}_{zz}(x,z_{\mathrm{a1}}=c_{\mathrm{a1}})=0 \tag{15}$$

$$\begin{aligned}V^{c}_{xx,x}(x)+\beta^{c}_1 b_{\mathrm{frp1}}\sigma^{\mathrm{a1}}_{zz}(x,z_{\mathrm{a1}}=0)\\ -\beta^{c}_2 b_{\mathrm{frp2}}\sigma^{\mathrm{a2}}_{zz}(x,z_{\mathrm{a2}}=c_{\mathrm{a2}})=-q_z(x)\end{aligned} \tag{16}$$

$$V^{\mathrm{frp2}}_{xx,x}(x)+\beta^{\mathrm{frp}}_2 b_{\mathrm{frp2}}\sigma^{\mathrm{a2}}_{zz}(x,z_{\mathrm{a2}}=0)=0 \tag{17}$$

$$\begin{aligned}M^{\mathrm{frp1}}_{xx,x}(x)-V^{\mathrm{frp1}}_{xx}(x)\\ +\alpha^{\mathrm{frp}}_1 b_{\mathrm{frp1}}\frac{d_{\mathrm{frp1}}}{2}\tau^{\mathrm{a1}}_{xz}(x,z_{\mathrm{a1}}=c_{\mathrm{a1}})=0\end{aligned} \tag{18}$$

$$\begin{aligned}M^{c}_{xx,x}(x)-V^{c}_{xx}(x)+\alpha^{c}_1 b_{\mathrm{frp1}}\frac{d_c}{2}\tau^{\mathrm{a1}}_{xz}(x,z_{\mathrm{a1}}=0)\\ +\alpha^{c}_2 b_{\mathrm{frp2}}\frac{d_c}{2}\tau^{\mathrm{a2}}_{xz}(x,z_{\mathrm{a2}}=c_{\mathrm{a2}})=m_x(x)\end{aligned} \tag{19}$$

$$\begin{aligned}M^{\mathrm{frp2}}_{xx,x}(x)-V^{\mathrm{frp2}}_{xx}(x)\\ +\alpha^{\mathrm{frp}}_2 b_{\mathrm{frp2}}\frac{d_{\mathrm{frp2}}}{2}\tau^{\mathrm{a2}}_{xz}(x,z_{\mathrm{a2}}=0)=0\end{aligned} \tag{20}$$

$$\tau^{\mathrm{a1}}_{xz,x}(x,z_{\mathrm{a1}})+\sigma^{\mathrm{a1}}_{zz,z}(x,z_{\mathrm{a1}})=0 \tag{21}$$

$$\tau^{\mathrm{a1}}_{xz,z}(x,z_{\mathrm{a1}})=0 \tag{22}$$

$$\tau^{\mathrm{a2}}_{xz,x}(x,z_{\mathrm{a2}})+\sigma^{\mathrm{a2}}_{zz,z}(x,z_{\mathrm{a2}})=0 \tag{23}$$

$$\tau^{\mathrm{a2}}_{xz,z}(x,z_{\mathrm{a2}})=0 \tag{24}$$

where N^i_{xx}, V^i_{xx}, and M^i_{xx} ($i=c,\mathrm{frp1},\mathrm{frp2}$) are the in-plane, shear, and the bending moment stress resultants in the masonry unit, the mortar joint, and the FRP strips; b_i ($i=\mathrm{frp1},\mathrm{frp2}$) is the width of the inner and outer FRP strips; α^n_m is a flag for the *bonding condition* at the inner ($m=1$) and outer ($m=2$) adhesive-FRP ($n=\mathrm{frp}$) and adhesive-masonry/mortar ($n=c$) interfaces, respectively, ($\alpha^n_m=1$ for a bonded interface; $\alpha^n_m=0$ for a debonded interface); β^n_m is a flag for the *contact conditions* at the debonded interface ($\beta^n_m=0$ for debonding without contact; $\beta^n_m=1$ for debonding with contact). The distinction between the masonry regions ($c=\mathrm{mu}$) and the mortar regions ($c=\mathrm{mj}$) is achieved through the constitutive relations that are discussed next.

2.3. Constitutive relations

Following the experimental findings reported in [8,15] and the tendency of the flexural cracks to develop at the

mortar joints only, it is assumed that the constitutive relations of the masonry units are linear elastic. On the other hand, the cracking of the mortar joints is considered. It is assumed that the behavior of the mortar material in compression and shear is linear elastic, and the only nonlinear effect is due to cracking. Thus, the constitutive relation for the normal stresses in the mortar is

$$\sigma_{xx}^{\mathrm{mj}} = \begin{cases} E_{\mathrm{mj}}\varepsilon_{xx}^{\mathrm{mj}} & \text{if } \varepsilon_{xx}^{\mathrm{mj}} \leqslant \varepsilon_{\mathrm{t}}^{\mathrm{mj}} \\ 0 & \text{if } \varepsilon_{xx}^{\mathrm{mj}} > \varepsilon_{\mathrm{t}}^{\mathrm{mj}} \end{cases} \tag{25}$$

where E_{mj} is the modulus of elasticity of the mortar, and $\varepsilon_{\mathrm{t}}^{\mathrm{mj}}$ is its the ultimate tensile or bond strain. The cross-sectional constitutive relations for the masonry units ($c = \mathrm{mu}$) and the mortar joints ($c = \mathrm{mj}$) are given by

$$\begin{aligned} N_{xx}^{c} &= A_{11}^{c}u_{oc,x} - B_{11}^{c}\phi_{c,x} \\ M_{xx}^{c} &= B_{11}^{c}u_{oc,x} - D_{11}^{c}\phi_{c,x} \\ V_{xx}^{c} &= A_{55}^{c}(w_{c,x} - \phi_{c}) \end{aligned} \tag{26a–c}$$

where A_{11}^{c}, B_{11}^{c}, D_{11}^{c} and A_{55}^{c} are the extensional, coupling, flexural, and shear rigidities of the masonry unit ($c = \mathrm{mu}$) or the mortar joint ($c = \mathrm{mj}$), multiplied by b_c, which is the width of the examined strengthened masonry strip [8,22].

The rigidities of the masonry units reduce to the traditional extensional, flexural and shear rigidities of the elastic masonry section and the coupling rigidity vanishes:

$$\begin{aligned} A_{11}^{\mathrm{mu}} &= EA_{\mathrm{mu}} \\ B_{11}^{\mathrm{mu}} &= 0 \\ D_{11}^{\mathrm{mu}} &= EI_{\mathrm{mu}} \\ A_{55}^{\mathrm{mu}} &= \kappa GA_{\mathrm{mu}} \end{aligned} \tag{27a–d}$$

where κ is the shear correction constant.

In the mortar joint, the nonlinear constitutive law and the combined in-plane and bending tractions require special consideration. The general stress and strain distributions under various combined tractions appear in Fig. 1(e). In case the tensile strains are lower than the ultimate tensile/bond strain $\varepsilon_{\mathrm{t}}^{\mathrm{mj}}$, the mortar joint is uncracked and the equivalent rigidities are given by Eq. (27) with "mj" instead of "mu". In case the tensile strains exceed $\varepsilon_{\mathrm{t}}^{\mathrm{mj}}$, the mortar joint is cracked and the equivalent rigidities take the following form:

$$\begin{aligned} A_{11}^{\mathrm{mj}} &= \int_{-d_{\mathrm{mj}}/2}^{z_{\mathrm{act}}^{\mathrm{mj}}} b_{\mathrm{mj}}E_{\mathrm{mj}}\mathrm{d}z_{\mathrm{mj}} = E_{\mathrm{mj}}b_{\mathrm{mj}}\left(\frac{d_{\mathrm{mj}}}{2} + \varphi z_{\mathrm{act}}^{\mathrm{mj}}\right) \\ B_{11}^{\mathrm{mj}} &= \int_{-d_{\mathrm{mj}}/2}^{z_{\mathrm{act}}^{\mathrm{mj}}} b_{\mathrm{mj}}E_{\mathrm{mj}}z_{\mathrm{mj}}\mathrm{d}z_{\mathrm{mj}} = -\varphi\frac{E_{\mathrm{mj}}b_{\mathrm{mj}}}{2}\left(\left(\frac{d_{\mathrm{mj}}}{2}\right)^{2} - \left(z_{\mathrm{act}}^{\mathrm{mj}}\right)^{2}\right) \\ D_{11}^{\mathrm{mj}} &= \int_{-d_{\mathrm{mj}}/2}^{z_{\mathrm{act}}^{\mathrm{mj}}} b_{\mathrm{mj}}E_{\mathrm{mj}}z_{\mathrm{mj}}^{2}\mathrm{d}z_{\mathrm{mj}} = \frac{E_{\mathrm{mj}}b_{\mathrm{mj}}}{3}\left(\left(\frac{d_{\mathrm{mj}}}{2}\right)^{3} + \varphi\left(z_{\mathrm{act}}^{\mathrm{mj}}\right)^{3}\right) \\ A_{55}^{\mathrm{mj}} &= \int_{-d_{\mathrm{mj}}/2}^{z_{\mathrm{act}}^{\mathrm{mj}}} b_{\mathrm{mj}}G_{\mathrm{mj}}\mathrm{d}z_{\mathrm{mj}} = \kappa G_{\mathrm{mj}}b_{\mathrm{mj}}\left(\frac{d_{\mathrm{mj}}}{2} + \varphi z_{\mathrm{act}}^{\mathrm{mj}}\right) \end{aligned} \tag{28a–d}$$

where b_{mj} and $z_{\mathrm{act}}^{\mathrm{mj}}$ are the width and the depth of the active zone in the mortar cross section, $\varphi = 1$ in case the mortar section is locally subjected to in-plane compression and a positive bending moment (Fig. 1(e)), $\varphi = -1$ in case of compression and a negative bending moment (Fig. 1(e)) and G_{mj} is the shear modulus of the mortar. In most practical cases, the contribution of the tensioned mortar to the stiffness of the cracked cross section is negligible (i.e. $\varepsilon_{\mathrm{t}}^{\mathrm{mj}} = 0$) and $z_{\mathrm{act}}^{\mathrm{mj}}$ can be replaced with z_{o}^{mj}, which is the depth of the compression zone.

The constitutive relations of the FRP strips follow the lamination theory and use Eqs. (26a–c) with "frp1" or "frp2" instead of "c". In this case, A_{11}^{i}, B_{11}^{i}, D_{11}^{i} and A_{55}^{i} ($i = \mathrm{frp1}, \mathrm{frp2}$) are the extensional, coupling, flexural, and shear rigidities of the FRP strips [23] multiplied by their width. The constitutive relations for the adhesive are

$$\sigma_{zz}^{j} = E_{j}\varepsilon_{zz}^{j}; \quad \tau_{xz}^{j} = G_{j}\gamma_{xz}^{j} \quad (j = \mathrm{a1}, \mathrm{a2}) \tag{29a, b}$$

where E_j and G_j ($j = \mathrm{a1}, \mathrm{a2}$) are the modulus of elasticity and the shear modulus of the adhesive material, respectively.

2.4. Adhesive layers – stress and displacement fields

The stress and displacement fields in the adhesive layers follow the high-order approach [20]. In the fully bonded regions, they are derived using Eqs. (21)–(24), along with the compatibility requirements (Eqs. (6)–(9)) and the kinematic and constitutive relations (Eqs. (4) and (29)), and take the following form:

$$\tau_{xz,z}^{j}(x, z_j) = \tau_{xz}^{j}(x) = \tau_j \tag{30}$$

$$\sigma_{zz}^{j}(x, z_j) = -\frac{2z_j - c_j}{2}\tau_{j,x} + \frac{\lambda E_j(w_i - w_c)}{c_j} \tag{31}$$

$$\begin{aligned} w_j(x, z_j) = &-\frac{z_j^2 - c_j z_j}{2E_j}\tau_{j,x} + \frac{\lambda(w_i - w_c)z_j}{c_j} \\ &+ \frac{(1+\lambda)}{2}w_c + \frac{(1-\lambda)}{2}w_{\mathrm{frp2}} \end{aligned} \tag{32}$$

$$\begin{aligned} u_j(x, z_j) = &\frac{\tau_j z_j}{G_j} + \frac{\tau_{j,xx}}{2E_j}\left(\frac{z_j^3}{3} - c_j\frac{z_j^2}{2}\right) - \frac{\lambda(w_{i,x} - w_{c,x})z_j^2}{2c_j} \\ &- \frac{(\lambda+1)}{2}\left(w_{c,x}z_{\mathrm{a1}} - u_{oc} + \frac{d_c}{2}\phi_c\right) \\ &+ \frac{(\lambda-1)}{2}\left(w_{\mathrm{frp2},x}z_{\mathrm{a2}} - u_{oc} + \frac{d_{\mathrm{frp2}}}{2}\phi_{\mathrm{frp2}}\right) \end{aligned} \tag{33}$$

where $\lambda = 1$ for $j = \mathrm{a1}$ and $i = \mathrm{frp1}$, and $\lambda = -1$ for $j = \mathrm{a2}$ and $i = \mathrm{frp2}$. The stress fields in the debonded sub-regions (with or without contact) are as follows:

$$\tau_{xz,z}^{j}(x, z_j) = \tau_{xz}^{j}(x) = \tau_j = 0 \tag{34}$$

$$\sigma_{zz}^{j}(x, z_j) = \frac{\beta_j^{c}\beta_j^{\mathrm{frp}}\lambda E_j(w_i - w_c)}{c_j} \tag{35}$$

2.5. Governing equations

The governing equations for the strengthened (fully bonded or debonded) regions are derived using Eqs.

(12)–(20), the constitutive relations (Eqs. (25)–(29)), the compatibility requirements (Eqs. (7b) and (9b)), and the stress and deformation fields of the adhesive layers (Eqs. (30)–(35)). The governing equations are generally stated in terms of the unknown displacements and rotations, $(w_c, w_{\mathrm{frp1}}, w_{\mathrm{frp2}}, u_{oc}, u_{o\mathrm{frp1}}, u_{o\mathrm{frp2}}, \phi_c, \phi_{\mathrm{frp1}}, \phi_{\mathrm{frp2}})$, and the unknown shear stresses (τ_{a1} and τ_{a2}), and read

$$A_{11}^{\mathrm{frp1}} u_{o\mathrm{frp1},xx} - B_{11}^{\mathrm{frp1}} \phi_{b,xx} - \alpha_1^{\mathrm{frp}} \alpha_1^c b_{\mathrm{frp1}} \tau_{\mathrm{a1}} = 0 \tag{36}$$

$$A_{11}^c u_{oc,xx} - B_{11}^c \phi_{c,xx} - \alpha_2^{\mathrm{frp}} \alpha_2^c b_{\mathrm{frp2}} \tau_{\mathrm{a2}} + \alpha_1^{\mathrm{frp}} \alpha_1^c b_{\mathrm{frp1}} \tau_{\mathrm{a1}} = -n_x \tag{37}$$

$$A_{11}^{\mathrm{frp2}} u_{o\mathrm{frp2},xx} - B_{11}^{\mathrm{frp2}} \phi_{\mathrm{frp2},xx} + \alpha_2^{\mathrm{frp}} \alpha_2^c b_{\mathrm{frp1}} \tau_{\mathrm{a2}} = 0 \tag{38}$$

$$A_{55}^{\mathrm{frp1}} (w_{\mathrm{frp1},xx} - \phi_{\mathrm{frp1},x}) + \frac{\alpha_1^{\mathrm{frp}} \alpha_1^c b_{\mathrm{frp1}} c_{\mathrm{a1}}}{2} \tau_{\mathrm{a1},x} - \beta_1^c \beta_1^{\mathrm{frp}} \frac{b_{\mathrm{frp1}} E_{\mathrm{a1}}}{c_{\mathrm{a1}}} (w_{\mathrm{frp1}} - w_c) = 0 \tag{39}$$

$$A_{55}^c (w_{c,xx} - \phi_{c,x}) + \frac{\alpha_2^{\mathrm{frp}} \alpha_2^c b_{\mathrm{frp2}} c_{\mathrm{a2}}}{2} \tau_{\mathrm{a2},x} + \frac{\alpha_1^{\mathrm{frp}} \alpha_1^c b_{\mathrm{frp1}} c_{\mathrm{a1}}}{2} \tau_{\mathrm{a1},x} + \beta_2^c \beta_2^{\mathrm{frp}} \frac{b_{\mathrm{frp2}} E_{\mathrm{a2}}}{c_{\mathrm{a2}}} (w_{\mathrm{frp2}} - w_c) + \beta_1^c \beta_1^{\mathrm{frp}} \frac{b_{\mathrm{frp1}} E_{\mathrm{a1}}}{c_{\mathrm{a1}}} (w_{\mathrm{frp1}} - w_c) = -q_z \tag{40}$$

$$A_{55}^{\mathrm{frp2}} (w_{\mathrm{frp2},xx} - \phi_{\mathrm{frp2},x}) + \frac{\alpha_2^{\mathrm{frp}} \alpha_2^c b_{\mathrm{frp2}} c_{\mathrm{a2}}}{2} \tau_{\mathrm{a2},x} - \beta_2^c \beta_2^{\mathrm{frp}} \frac{b_{\mathrm{frp2}} E_{\mathrm{a2}}}{c_{\mathrm{a2}}} (w_{\mathrm{frp2}} - w_c) = 0 \tag{41}$$

$$D_{11}^{\mathrm{frp1}} \phi_{\mathrm{frp1},xx} - B_{11}^{\mathrm{frp1}} u_{o\mathrm{frp1},xx} + A_{55}^{\mathrm{frp1}} (w_{\mathrm{frp1},x} - \phi_{\mathrm{frp1}}) - \alpha_1^{\mathrm{frp}} \alpha_1^c b_{\mathrm{frp1}} \frac{d_{\mathrm{frp1}}}{2} \tau_{\mathrm{a1}} = 0 \tag{42}$$

$$D_{11}^c \phi_{c,xx} - B_{11}^c u_{oc,xx} + A_{55}^c (w_{c,x} - \phi_c) - \alpha_2^{\mathrm{frp}} \alpha_2^c b_{\mathrm{frp2}} \frac{d_c}{2} \tau_{\mathrm{a2}} - \alpha_1^{\mathrm{frp}} \alpha_1^c b_{\mathrm{frp1}} \frac{d_c}{2} \tau_{\mathrm{a1}} = -m_x \tag{43}$$

$$D_{11}^{\mathrm{frp2}} \phi_{\mathrm{frp2},xx} - B_{11}^{\mathrm{frp2}} u_{o\mathrm{frp2},xx} + A_{55}^{\mathrm{frp2}} (w_{\mathrm{frp2},x} - \phi_{\mathrm{frp2}}) - \alpha_2^{\mathrm{frp}} \alpha_2^c b_{\mathrm{frp2}} \frac{d_{\mathrm{frp2}}}{2} \tau_{\mathrm{a2}} = 0 \tag{44}$$

$$\alpha_1^{\mathrm{frp}} \alpha_1^c \left(u_{oc} - u_{o\mathrm{frp1}} - \frac{c_{\mathrm{a1}}}{2} (w_{\mathrm{frp1},x} + w_{c,x}) + \frac{\tau_{\mathrm{a1}} c_{\mathrm{a1}}}{G_{\mathrm{a1}}} - \frac{\tau_{\mathrm{a1},xx} c_{\mathrm{a1}}^3}{12 E_{\mathrm{a1}}} - \frac{d_{\mathrm{frp1}}}{2} \phi_{\mathrm{frp1}} - \frac{d_c}{2} \phi_c \right) = 0 \tag{45}$$

$$\alpha_2^{\mathrm{frp}} \alpha_2^c \left(u_{o\mathrm{frp2}} - u_{oc} - \frac{c_{\mathrm{a2}}}{2} (w_{\mathrm{frp2},x} + w_{c,x}) + \frac{\tau_{\mathrm{a2}} c_{\mathrm{a2}}}{G_{\mathrm{a2}}} - \frac{\tau_{\mathrm{a2},xx} c_{\mathrm{a2}}^3}{12 E_{\mathrm{a2}}} - \frac{d_{\mathrm{frp2}}}{2} \phi_{\mathrm{frp2}} - \frac{d_c}{2} \phi_c \right) = 0 \tag{46}$$

Eqs. (45) and (46) result from the in-plane compatibility conditions, Eqs. (7b) and (9b). Thus, they are valid in the fully bonded sub-regions and vanish in the debonded ones.

2.6. Boundary and continuity conditions

The boundary conditions for the masonry panel, the FRP strips, and the adhesive layers are

$$\psi N_{xx}^i = \vartheta N_k \quad \text{or} \quad u_{oi} = \bar{u}_{oi} \tag{47}$$

$$-\psi M_{xx}^i = \vartheta M_k \quad \text{or} \quad \phi_i = \bar{\phi}_i \tag{48}$$

$$\psi V_{xx}^i = \vartheta P_k \quad \text{or} \quad w_i = \bar{w}_i \tag{49}$$

$$\tau_j = 0 \quad \text{or} \quad w_j(z_j) = \bar{w}_j(z_j) \tag{50}$$

where P_k, N_k and M_k are external loads and bending moments at $x_k = 0$ or $x_k = L$; the over-bar designates prescribed deformations or rotations; $\psi = 1$ where $x = H$; $\psi = -1$ where $x = 0$; $\vartheta = 1$ for the boundary conditions of the masonry units or the mortar joints; and $\vartheta = 0$ for the boundary conditions of the FRP strips.

The continuity conditions at any point $x = x_k$ within the fully bonded sub-region are ($i = c, \mathrm{frp1}, \mathrm{frp2}$)

$$u_{oi}^{(-)} = u_{oi}^{(+)}; \quad w_i^{(-)} = w_i^{(+)}; \quad \phi_i^{(-)} = \phi_i^{(+)} \tag{51a–c}$$

$$N_{xx}^{i(-)} - N_{xx}^{i(+)} = \vartheta N_k; \quad -M_{xx}^{i(-)} + M_{xx}^{i(+)} = \vartheta M_k;$$

$$V_{xx}^{i(-)} - V_{xx}^{i(+)} = \vartheta P_k \tag{52a–c}$$

$$\tau_j^{(-)} = \tau_j^{(+)}; \quad w_j^{(-)}(z_j) = w_j^{(+)}(z_j) \tag{53a–b}$$

where the $(-)$ and $(+)$ superscripts denote quantities left and right to the point $x = x_k$, respectively. The continuity conditions within a debonded sub-region include Eqs. (51) and (52) only. The continuity conditions at the mutual point between a fully bonded sub-region and a debonded one include Eqs. (51) and (52) along with the requirement of zero shear stress in the fully bonded sub-region at the connection point.

2.7. Solution procedure

The governing equations are associated with nonlinearity due to the unknown type of debonded sub-regions (with or without out-of-plane contact) and due to cracking of the mortar joints. The type of debonded sub-regions is determined iteratively. Namely, one type is assumed and verified through the results of the analysis. If the results contradict the assumption, the assumed type of the debonded region is switched and the structure is reanalyzed. The nonlinearity associated with the cracking of the mortar joints is considered through the following iterative procedure:

Step 1: Initial guess.
All mortar joints are assumed uncracked.

Step 2: Analysis of the structure.
Using the rigidities calculated in the initial guess or in the previous iteration, the governing equations become linear ordinary differential equations with constant coefficients. In this case, they can be solved analytically or numerically using standard procedures (finite difference, collocations, etc.), or using BVP solvers available in packages such as Maple or Matlab. Here, a multiple shooting numerical procedure [24] is adopted.

Step 3: Analysis of the mortar joints cross-section.
Based on the solution obtained in step 2, the depth of the compression zone in each cracked joint is determined:

Step 3.1: The strain distribution in each mortar joint is determined through Eq. (3d).

Step 3.2: In each *cracked* joint, the depth of the active zone is determined as follows:

$$z_{\text{act}}^{\text{mj}} = \frac{u_{o\text{mj},x}}{\phi_{\text{mj},x}} - \frac{\varepsilon_{\text{t}}^{\text{mj}}}{\phi_{\text{mj},x}} \tag{54}$$

where $u_{o\text{mj},x}$ and $\phi_{\text{mj},x}$ are obtained in step 2.

Step 3.3: Once $z_{\text{act}}^{\text{mj}}$ is determined, the rigidities of each joint are evaluated using Eq. (30). Due to the relatively small height of the joints (with respect to the height of the wall), it is assumed that the rigidities are uniform through the height of each joint.

Step 4: Convergence criterion.

If the norm of the relative difference between the magnitudes of the equivalent rigidities of the mortar joints in two successive iterations is sufficiently small, the iterative procedure is stopped. Otherwise, the procedure returns to step 2 with the updated rigidities determined in step 3.

Note that once the mortar joint is cracked, the stresses due to the self-weight of the wall are redistributed and are partially transferred to the bonded FRP strips. Following the concepts commonly used in the analysis of prestressed concrete structures [25], it is assumed that the self-weight is exerted on the strengthened section.

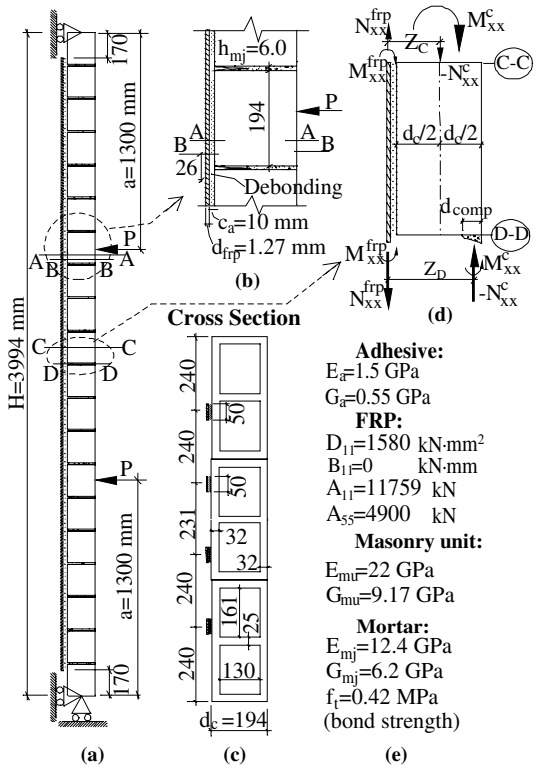

Fig. 2. Geometry, material properties, loading, and moment resistance mechanisms: (a) geometry and loading scheme; (b) cracked mortar joint and debonded regions; (c) cross section; (d) moment resistance mechanisms; (e) mechanical properties.

3. Numerical study

The numerical study aims to reveal the capabilities of the model, to clarify the interaction between the variables, and to explore some of the aspects of the response of the strengthened wall. The geometry of the wall, the strengthening scheme, and the loading scheme follow the experimental study of [12] and appear in Fig. 2. The mechanical properties of the concrete masonry units and the type S mortar follow [26], and $\varepsilon_{\text{t}}^{\text{mj}}$ is defined based on the bonding strength of the mortar and follows [27]. In the uncracked stage, the FRP strips are assumed to be fully bonded. Yet, once the joint is cracked, it is assumed that due to the crack opening and to the inability of the cracked faces to transfer shear stresses, a debonded region is formed. The height of each debonded region is estimated as the height of the mortar joint plus twice the thickness of the adhesive layer (see Fig. 2(b)). Also, following the experimental observations reported in [12], the effective width of the masonry strip reduces to the overall width of the strengthening system due to the cracking of the face shell of the hollow masonry unit.

The analytically predicted and experimentally observed load–deflection response of the strengthened wall and the analytical distributions of the deformations, internal forces, and stresses under the self weight ($n_x = 0.372$ kN/m) and a lateral load of 30 kN are described in Figs. 3 and 4. The load–deflection curves (Fig. 3(a)) reveal fair agreement between the theoretical and the actual responses up to about 20 kN. At higher load levels, the analytical prediction deviates from the experimental one due to further damage accumulation. The response under low levels of load shows that the joints in the constant moment region crack simultaneously and lead to a considerable reduction in the stiffness. The cracking of the joints in the shear spans has a smaller influence. The experimental study [12] showed that the unstrengthened masonry wall failed under load and deflection levels of about 1 kN and 0.7 mm, respectively, while the strengthened wall failed under 46.4 kN. The improved behavior of the strengthened wall and its ability to resist load beyond the cracking point are well reflected by the analytical model.

Fig. 3(b) describes the deflection curve achieved by the analytical model derived here and by a simple bending model with cracked masonry section properties. The results show that the simple model predicts larger deflections than those detected by the present model. This is attributed to the concentration of the cracking in the mortar joints and to the ability of the masonry unit between the joints to resist bending. This type of behavior is not accounted for by the simple cracked section bending analysis.

The longitudinal deformations at the reference line level (detected by the analytical model derived here) appear in Fig. 3(c), and reveal "jumps" across the cracked mortar

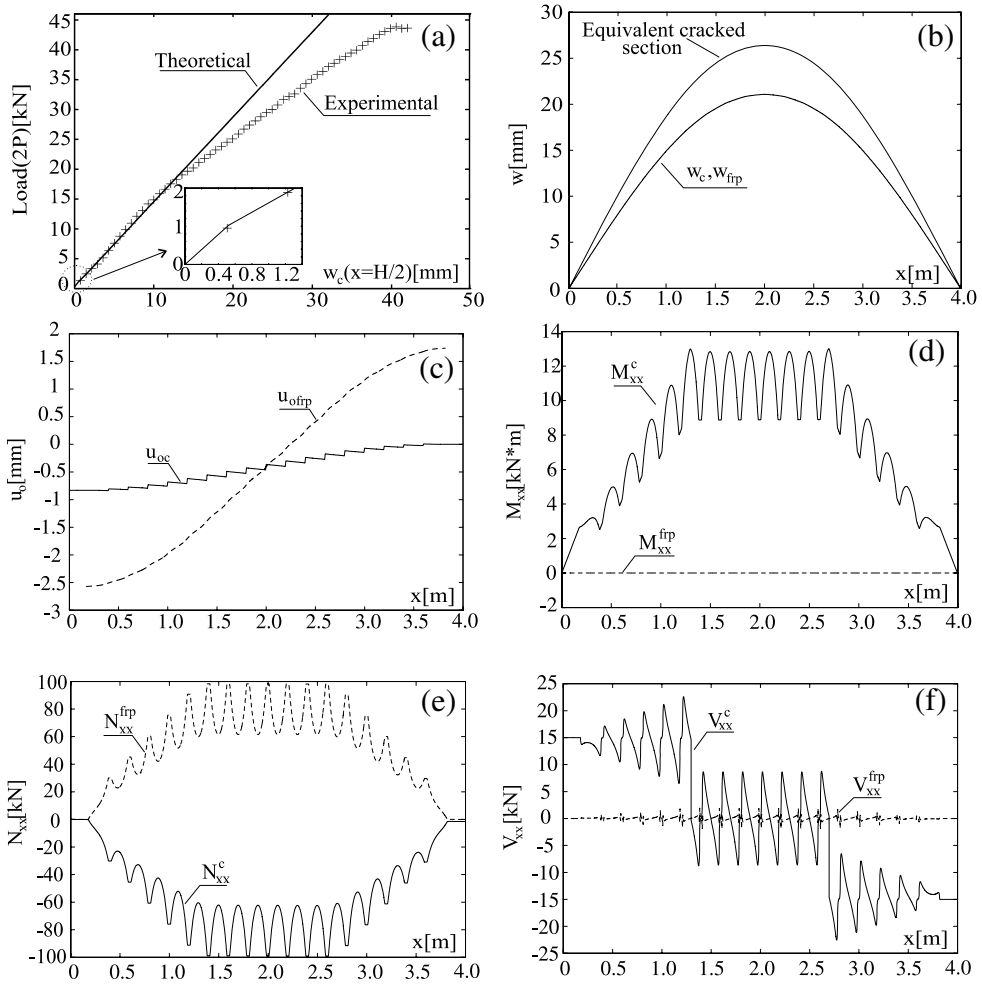

Fig. 3. Load–deflection curves and response of the strengthened wall under $P = 15$ kN and self weight: (a) load–deflection behavior; (b) out-of-plane deflections; (c) longitudinal deformations; (d) bending moments; (e) axial forces; (f) shear forces.

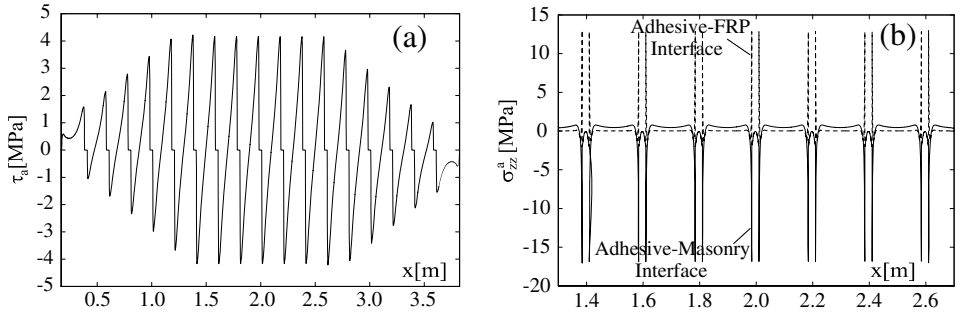

Fig. 4. Stresses in the adhesive layer: (a) shear stresses; (b) out-of-plane normal stresses.

joints. This type of behavior cannot be described by the simple bending model. Furthermore, the results clarify that the cracked joints and the associated "jumps" are spread along the height of the wall and are not limited to the mid-height joint only, which is the case in the un-strengthened masonry wall.

The analytically predicted distributions of the bending moments and the axial forces appear in Figs. 3(d) and (e), respectively. These results are highly affected by the dramatic change of the stiffness between the masonry unit section and the cracked mortar joint section. In the cracked mortar joint, the axial forces are increased and the bending moment carried by the masonry panel (plotted with respect to the mid-height reference line) is decreased. These observations are in agreement with the experimental findings reported in [28]. In the masonry unit section between adja-

cent joints, the increased flexural stiffness of the masonry unit allows a larger portion of the global moment to be carried by the masonry unit itself. As a result, the part of the global moment carried through tension in the FRP strip and compression in the wall (the "composite action" moment) is reduced.

The distributions of the shear forces in the masonry panel and the FRP strips obtained by the analytical model are described in Fig. 3(f). It is seen that the variation of the moment resistance mechanism through the height of the wall yield localized shear forces near the edges of the masonry units. The magnitudes of the localized shear forces, which are also observed in zone with zero global shear, are of the same order as the peak global shear forces. The concentrated shear forces near the cracked joints may be associated with shear cracking of the masonry units, shear sliding of the masonry units (mortar slip), or shear failure of the joint, see [11,12,14].

The analytically predicted shear and peeling stresses in the adhesive layer are studied in Fig. 4. The results reveal that the rapid variation and sign reversal of the shear stress along the masonry units result in high shear gradients, and consequently, in high out-of-plane normal (peeling) stresses (see Eq. (31)). The development of these stress concentrations near the mortar joints quantitatively explains the debonding failure mechanism that has been observed in many experimental studies [8,9,11,15].

3.1. Parametric study

The interaction between some of the variables and their influence on the response of the wall are studied through a parametric study. The geometry, properties, and loading scheme appear in Fig. 2, yet, the hollow masonry units are replaced with solid ones. Correspondingly, following [21,22], the effective width of the masonry panel is taken as the entire width of the wall. The load level is 30 kN ($P = 15$ kN) and reference results obtained using the data given in Fig. 2 are marked with the symbol "o".

The response of the wall is examined in terms of the maximum out-of-plane deflection at midspan, the peak shear forces, $V^{c}_{xx,\max}$ and $V^{\mathrm{frp}}_{xx,\max}$ (normalized with respect to the global shear force), and the shear and peeling stresses in the adhesive interfaces at their critical locations near the loading point (section A–A "$x = x_A$" and B–B "$x = x_B$" in Fig. 2). The magnitude of the bending moment carried in the form of a force couple (the "composite action" moment) normalized with respect to the global bending moment in the section is also studied. This value is examined in the masonry units section (section C–C in Fig. 2) and the cracked joint section (section D–D in Fig. 2), and reflects the load carrying mechanism in the different sections.

The effect of the modulus of elasticity of the masonry unit and the corresponding shear modulus (determined using Poisson's ratio of 0.2) on the behavior of the strengthened masonry wall is described in Fig. 5. The case of infinitely rigid masonry units [29,30] is also investigated. Fig. 5 indicates that opposed to their notable effect on the elastic response of the wall [17], the influence of the elastic properties of the masonry units on the inelastic (post-cracking) response of the masonry wall is not significant. The results also show that modeling the masonry units as rigid bodies may be adopted in order to reduce the computational efforts and to simplify the analysis.

The effect of the elastic moduli of the FRP strips on the behavior of the strengthened wall is described in Fig. 6. The results quantitatively reveal a notable reduction of the out-of-plane deflection due to the stiffening of the FRP strips (Fig. 6(a)). On the other hand, the level of the composite action observed at the strengthened mortar joint section (D–D) is not affected by the modulus of the FRP strips (Fig. 6(b)). This is attributed to the negligible bending moment carried by the cracked mortar itself. As a result, the tensile force in the FRP reinforcement is mainly determined through equilibrium of moments in this section, independently of the stiffness parameters. The level of the composite action in the masonry unit (section C–C) increases with the increase of the stiffness of the FRP strips, whereas the maximum shear forces and the shear and peeling stresses at the adhesive decrease. In order to explain this phenomenon, the distributions of the axial forces in

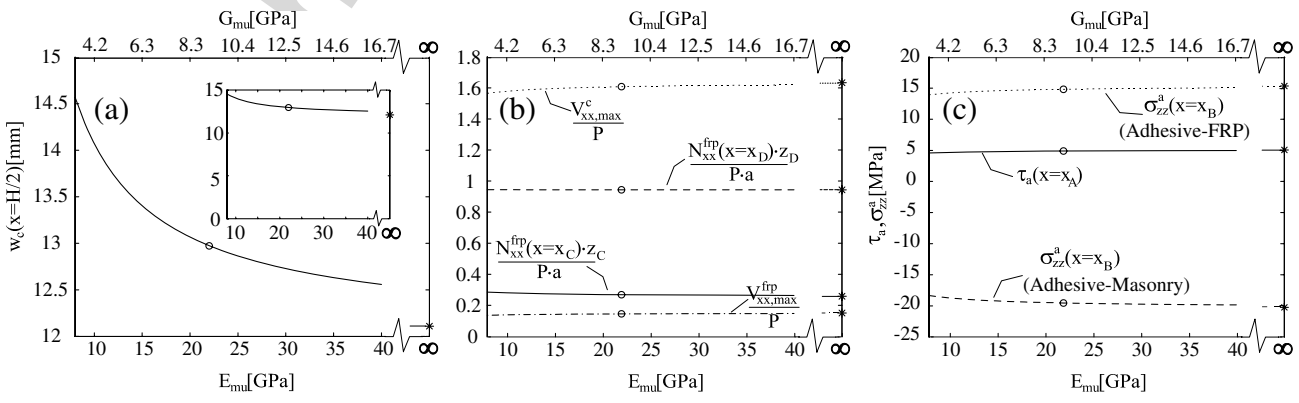

Fig. 5. Influence of the elastic and shear moduli of the masonry units on the behavior of the strengthened wall: (a) out-of-plane deflections; (b) axial forces in sections C–C and D–D and maximum shear forces; (c) shear and out-of-plane normal stresses in sections A–A and B–B.

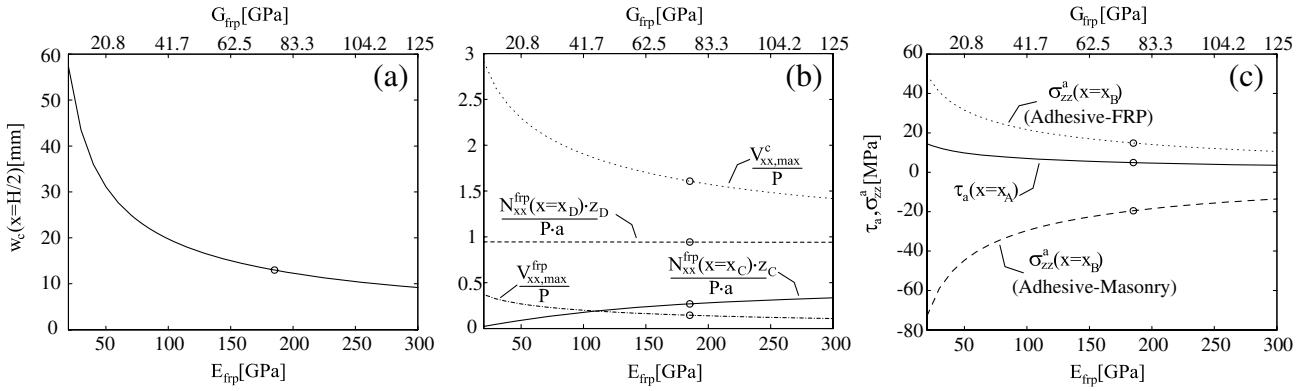

Fig. 6. influence of the mechanical properties of the FRP strip on the behavior of the strengthened wall: (a) out-of-plane deflections; (b) axial forces in sections C–C and D–D and maximum shear forces; (c) shear and out-of-plane normal stresses in sections A–A and B–B.

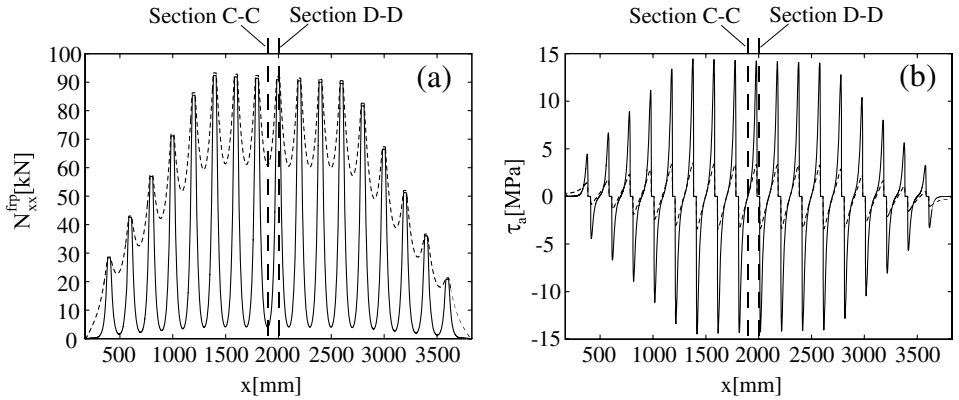

Fig. 7. Distribution of the axial force in the FRP reinforcement (total in all four strips) and the shear stress in the adhesive through the height of the masonry panel: (a) axial force; (b) shear stress. (Legend: (—) $E_{frp} = 20$ GPa, (---) $E_{frp} = 300$ GPa).

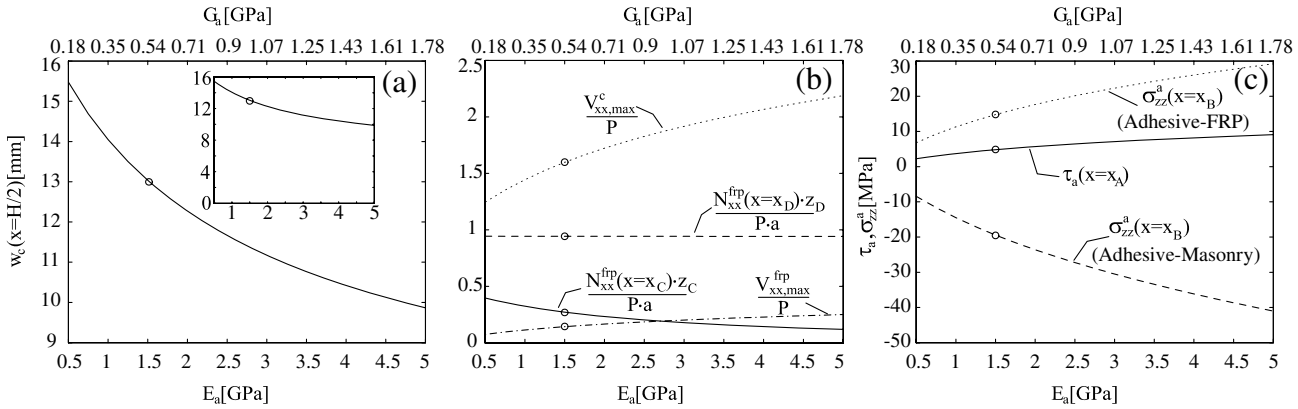

Fig. 8. Influence of the mechanical properties of the adhesive on the behavior of the strengthened wall: (a) out-of-plane deflections; (b) axial forces in sections C–C and D–D and maximum shear forces; (c) shear and out-of-plane normal stresses in sections A–A and B–B.

the FRP reinforcement and the shear stresses obtained with $E_{frp} = 20$ GPa and $E_{frp} = 300$ GPa appear in Fig. 7. These results show that in the masonry unit section (C–C), the tensile force in the compliant FRP strips ($E_{frp} = 20$ GPa) is much smaller than the one obtained with stiffer strips ($E_{frp} = 300$ GPa). On the other hand, the axial force in the joint section (D–D) is not affected by E_{frp}, see Fig. 7(a). The variation between section C–C and D–D is achieved through shear stressing of the adhesive, see Fig. 7(b). Hence, the magnitudes of the interfacial shear stresses in the adhesive layer decrease with the increase in the tensile force in section C–C. Correspondingly, the shear

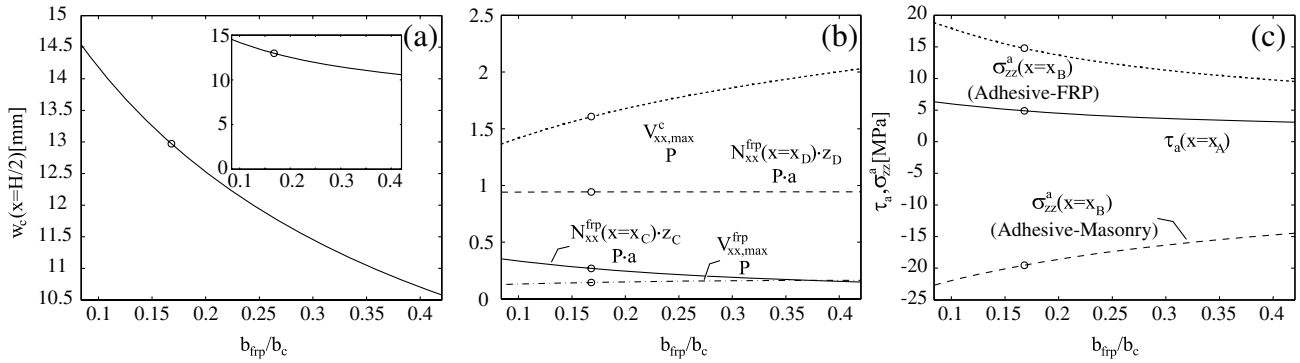

Fig. 9. Influence of the coverage ratio of the strengthening system on the behavior of the strengthened wall: (a) out-of-plane deflections; (b) axial forces in sections C–C and D–D and maximum shear forces; (c) shear and out-of-plane normal stresses in sections A–A and B–B.

gradients and the magnitudes of the out-of-plane stresses also decrease, (see Fig. 6(c) and Eq. (31)).

The effect of the elastic moduli of the adhesive layers on the behavior of the strengthened masonry wall is studied in Fig. 8. Fig. 8(a) shows that increasing the elastic moduli of the adhesive leads to a notable reduction of the out-of-plane deflections of the wall. This result is mainly an outcome of increasing the shear rigidity of the adhesive, which improves the stress transfer mechanism between the masonry units and the FRP reinforcement and allows a more effective reduction of the tensile forces in the FRP reinforcement in section C–C (Fig. 8(b)). On the other hand, the stiffening of the adhesive material increases the magnitudes of the interfacial stresses in the adhesive (Fig. 8(c)), and amplifies the localized shear effects in the masonry units and the FRP strips (Fig. 8(b)).

The influence of the FRP coverage ratio (b_{frp}/b_c) is studied in Fig. 9. The results in Fig. 9(a) show that increasing the FRP coverage ratio (while keeping its total cross-sectional area constant) results in a reduction of the out-of-plane deflections. This result is attributed to the large bonding area that allows a more effective stress transfer mechanism. Fig. 9(c) reveals a reduction in the shear and out-of-plane normal stresses. Hence, increasing the coverage ratio improves the structural performance and reduces the vulnerability of the strengthened wall to the debonding modes of failures. This observation is also reflected by the experimental study reported in [1].

4. Summary and conclusions

A theoretical model for the structural analysis of the out-of-plane bending behavior of unreinforced masonry walls strengthened with FRP strips has been presented. The mathematical model accounts for the layered layout of the strengthened wall and for the unique nonlinear phenomena associated with the cracking of the joints.

The capabilities of the theoretical model have been demonstrated through a numerical example. The numerical results have shown that the considerable difference between the flexural stiffness of the masonry unit and that of the cracked mortar joint significantly affect the distribution of the internal forces in the FRP strips and in the masonry panel. These effects cannot be detected using simple strain compatibility or homogenization approaches. Along with the global effects, the localized shear forces that develop in the FRP strip near the edges of the joint, and the development of concentrated shear and tensile out-of-plane normal (peeling) stresses in the adhesive near the corners of the masonry unit have been revealed. These stress concentrations provide a quantitative explanation for the debonding failure mechanisms that have been observed in many experimental studies.

The influence of some of the properties of the strengthened wall on the overall and the localized response have been parametrically studied. The results have shown that the use of stiffer FRP strips tends to decrease the out-of-plane deflection, the internal shear and axial forces in the masonry unit and the FRP strips, and the shear and peeling stresses in the adhesive. The behavior of the strengthened wall is also affected by the elastic properties of the adhesive and by the coverage ratio of the external FRP reinforcement. On the other hand, in the case studied here, the elastic properties of the masonry units have a negligible influence on the post-cracking behavior of the wall.

In conclusion, the analytical model developed here sets a theoretical platform for the analysis of the strengthened masonry wall. This platform and the quantitative description of the physical phenomena clarify the response of the strengthened masonry wall and throw light on its unique structural behavior.

References

[1] Ehsani MR, Saadatmanesh H, Velazquez-Dimas JI. Behavior of retrofitted URM walls under simulated earthquake loading. J Compos Constr 1999;3(3):134–42.
[2] Triantafillou TC. Strengthening of masonry structures using epoxy-bonded FRP laminates. J Compos Constr 1998;2(2):96–104.
[3] Hamoush SA, McGinley MW, Mlakar P, Scott D, Murray K. Out-of-plane strengthening of masonry walls with reinforced composites. J Compos Constr 2001;5(3):139–45.
[4] Gilstrap JM, Dolan CW. Out-of-plane bending of FRP-reinforced masonry walls. Compos Sci Technol 1998;58(8):1277–84.

[5] Spadea G, Bencardino F, Swamy RN. Structural behavior of composite RC beams with externally bonded CFRP. J Compos Constr 1998;2(3):132–7.
[6] Buyukozturk O, Gunes O, Karaca E. Progress on understanding debonding problems in reinforced concrete and steel members strengthened with FRP composites. Constr Build Mater 2004;18(1):1–19.
[7] Ghobarah A, El Mandooh Galal K. Out-of-plane strengthening of unreinforced masonry walls with openings. J Compos Constr 2004;8(4):298–305.
[8] Hamilton HR, Dolan CW. Flexural capacity of glass FRP strengthened concrete masonry walls. J Compos Constr 2001;5(3):170–8.
[9] Kiss RM, Kollar LP, Jai J, Krawinkler H. Masonry strengthened with FRP subjected to combined bending and compression, Part II: Test results and model predictions. J Compos Mater 2002;36(9):1049–63.
[10] Hamoush SA, McGinley MW, Mlakar P, Terro MJ. Out-of-plane behavior of surface-reinforced masonry walls. Constr Build Mater 2002;16(6):341–51.
[11] Tumialan JG, Galati N, Nanni A. Fiber-reinforced polymer strengthening of unreinforced masonry walls subjected to out-of-plane loads. ACI Struct J 2003;100(3):321–9.
[12] Albert ML, Elwi AE, Roger Cheng JJ. Strengthening of unreinforced masonry walls using FRPs. J Compos Constr 2001;5(2):76–84.
[13] Kuzik MD, Elwi AE, Cheng JJR. Cyclic flexure tests of masonry walls reinforced with glass fiber reinforced polymer sheets. J Compos Constr 2003;7(1):20–30.
[14] Davidson JS, Fisher JW, Hammons MI, Porter JR, Dinan RJ. Failure mechanisms of polymer-reinforced concrete masonry walls subjected to blast. J Struct Eng 2005;131(8):1194–205.
[15] Velazquea-Dimas JI, Ehsani MR. Modeling out-of-plane behavior of URM walls retrofitted with fiber composites. J Compos Constr 2000;4(4):172–81.
[16] Kiss RM, Kollar LP, Jai J, Krawinkler H. FRP strengthened masonry beams, Part I: Model. J Compos Mater 2002;36(5):521–36.
[17] Cecchi A, Milani G, Tralli A. Out-of-plane loaded CFRP reinforced masonry walls: mechanical characterization by homogenization procedure. Compos Sci Technol 2005;65(10):1480–500.
[18] Hamed E, Rabinovitch O. Out-of-plane bending of URM walls strengthened with FRP strips – modeling and analysis. In: Proceedings of the 7th international symposium on fiber reinforced polymer (FRP) reinforcement for concrete structures, Kansas City, MO, November 6–9, 2005. p. 249–68.
[19] Timoshenko S, Goodier JN. Theory of elasticity. 3rd ed. New York, NY: McGraw-Hill Book Co. Inc.; 1970.
[20] Rabinovitch O, Frostig Y. Closed-form high-order analysis of RC beams strengthened with FRP strips. J Compos Constr 2000;4(2):65–74.
[21] International Conference of Building Officials. Uniform Building Code, 1991 ed. Whittier, Calif, 1991.
[22] Foraboschi P. Strengthening of masonry arches with fiber-reinforced polymer strips. J Compos Constr 2004;8(3):191–202.
[23] Vinson JR, Sierakowski RL. The behavior of structures composed of composite materials. Dordrecht, The Netherlands: Martinus-Nijhoff; 1986.
[24] Stoer J, Bulirsch R. Introduction to numerical analysis. New York: Springer-Verlag; 1993.
[25] Weigel JA, Seguirant SJ, Brice R, Khaleghi B. High performance precast, pretensioned concrete girder bridges in Washington state. PCI J 2003;48(2):28–52.
[26] Fahmy EH, Ghoneim TGM. Behavior of concrete block masonry prisms under axial compression. Can J Civ Eng 1995;22(5):898–915.
[27] Laska WA, Ostrander CW, Nelson RL, Munro CC. Research of physical properties of masonry assemblages using regional materials. In: Matthys John H, editor. Masonry: components to assemblages. ASTM STP 1063. Philadelphia: American Society for Testing and Materials; 1990. p. 339–49.
[28] Roko K, Boothby TE, Bakis CE. Failure modes of sheet bonded fiber reinforced polymer applied to brick masonry. In: Dolan CW, Rizkalla SH, Nanni A, editors. 4th international symposium on fiber reinforced polymer (FRP) reinforcement for concrete structures (FRPRCS-4). Farmington Hills, Michigan: ACI; 1999. p. 305–11.
[29] Casolo S. Modeling the out-of-plane seismic behavior of masonry walls by rigid elements. Earthquake Eng Struct Dyn 2000;29(12):1797–813.
[30] Rabinovitch O, Hamed E. Bending behavior of sandwich panels with a "soft" core and embedded rigid inserts. In: 7th international conference on sandwich structures, Aalborg, Denmark, August 29–31, 2005.